

# A NON-TRADITIONAL VARIANT NONLINEAR ENERGY SINK: HARMONICALLY FORCED RESPONSES

Youzuo Jin<sup>1</sup>, Kefu Liu<sup>1</sup>, Liuyang Xiong<sup>2</sup>, Lihua Tang<sup>2</sup>

<sup>1</sup>Department of Mechanical Engineering, Lakehead University, Thunder Bay, Canada

<sup>2</sup>Department of Mechanical Engineering, University of Auckland, Auckland, New Zealand

**Abstract**—This study focuses on simultaneous vibration suppression and energy harvesting in a broad frequency band. For this purpose, a variant nonlinear energy sink (NES) is developed. The developed variant NES consists of a nonlinear oscillator and an electromagnetic energy harvester. Unlike a true NES, the nonlinear oscillator's spring is not essentially nonlinear. The variant NES is attached to a single-degree-of-freedom (SDOF) primary system that is subjected to a base excitation. Different from the traditional way, the electromagnetic energy harvester is placed between the oscillator's mass and the base. This study investigates the performance of this non-traditional variant NES under harmonic base excitation. First, the developed apparatus is described. Subsequently, the approximate solutions of steady state responses are derived using the harmonic balance (HB) method. Next, computer simulations are conducted using both the HB method's solution and numerical integration. The results show that under harmonic excitation, the proposed apparatus behaves similarly to a true NES with the following features: amplitude jump, excitation level dependence, strongly modulated response (SMR), etc. Overall, the non-traditional variant NES can achieve vibration suppression and energy harvesting in a broad frequency band.

**Keywords**—*nonlinear energy sink; energy harvesting; vibration suppression; harmonic excitation; harmonic balance method; frequency response plot*

## I. INTRODUCTION

In recent years, there has been a growing interest in harvesting energy from ambient vibration for self-powered devices. A popular way to convert vibrating energy into electricity is to use a single-degree-of-freedom (SDOF) oscillator. However, its performance will be compromised if the ambient vibration is not sinusoidal or the harmonic excitation frequency varies from the natural frequency of the oscillator. In order to widen the bandwidth, various nonlinear energy harvesters have been proposed [1, 2]. On the other hand, vibration absorbers consisting of an SDOF oscillator have been used to suppress vibration of a primary system subjected to a harmonic excitation. In terms of vibration suppression, linear vibration absorbers have a narrow working bandwidth.

Nonlinear vibration absorbers have been proposed to improve performance robustness in a broad frequency band [3-5]. Over the last two decades, the nonlinear energy sink (NES) has been considered to be a better solution for broadband vibration suppression [6-8]. The NES consists of a mass, a nonlinear spring, and a damper. Unlike the nonlinear vibration absorbers, the NES's spring is essentially nonlinear so that it can respond to any frequency as long as the excitation energy exceeds the required threshold [9].

Recently some studies have been conducted to explore the possibility of using the NES to suppress vibration and harvest energy simultaneously [10, 11]. Achieving an ideal NES requires stringent conditions. A common way is to connect a small mass between two aligned linear springs with no pretension. Various methods were used to eliminate the requirement of pretension, including using an air track or a guide rail to support the NES mass [12-14]. In [15-17], the apparatuses with high nonlinear stiffness and low linear stiffness were developed to emulate the performance of an ideal NES. These devices were referred to as variant NES. The studies showed that as long as the variant NES is weakly coupled to the primary system, it demonstrates the similar behaviors of an ideal NES, such as 1:1 resonance, targeted energy transfer (TET), and strongly modulated response (SMR).

In [18], a non-traditional vibration absorber was developed for the purpose of simultaneous vibration suppression and energy harvesting. The developed vibration absorber is considered to be non-traditional because its damper is connected between the absorber mass and the ground. In [19], a non-traditional variant NES was developed for broadband applications, and its performance under transient responses was examined. This paper investigates the performance of the non-traditional variant NES under harmonic excitation with the purpose of achieving simultaneous vibration suppression and energy harvesting.

The rest of the paper is organized as follows. Section II presents the developed apparatus and its modeling. Section III introduces the harmonic balance (HB) method that is used to find the approximate steady-state responses of the system. Section IV gives the computer simulation results. Section V draws the conclusion of the study.

## II. APPARATUS AND MODELING

Fig. 1 compares the two ways to attach a variant NES's damper. Fig. 1(a) is the traditional way named as variant NES model A while Fig. 1(b) is the non-traditional way named as variant NES model B. The non-traditional attachment offers some unique features in terms of applications and dynamics. For example, this way makes installation of a damper possible if the space between the NES mass and the primary mass is limited and the damper requires a large motion stroke.

Fig. 2 shows an isometric view and a front view of the developed apparatus which consists of a primary system attached by the proposed variant NES model B. The primary system is constructed by clamping a Poly-lactic Acid (PLA) block printed by a 3-D printer and a base plate with four thin steel plates. The variant NES model B consists of a steel cantilever beam, two continuous-contact blocks, two permanent magnets, and two coils that are fixed to the base plate. The continuous-contact blocks are also made of PLA filament by a 3-D printer. The upper end of the cantilever beam is clamped between the two continuous-contact blocks that are inserted in the primary block. The two magnets are attached to the free end of the cantilever beam by their own magnetic forces. As shown in Fig. 2, portions of the magnets are situated inside the coils such that they form two electromagnetic energy harvesters. Obviously, the developed apparatus represents a variant NES model B as the electromagnetic energy harvesters are connected between the NES mass and the base.

Fig. 3 is a schematic diagram showing the dynamic model of the developed apparatus.  $m_a$  and  $m_p$  stand for the NES mass and the primary mass, respectively.  $k_1$ ,  $k_3$ , and  $k_p$  represent the NES linear stiffness, the NES nonlinear stiffness, and the primary stiffness, respectively.  $c_{am}$ ,  $c_{ae}$ , and  $c_p$  represent the mechanical damping coefficient between the NES mass and the primary mass, the electric damping coefficient between the NES mass and the primary mass, and the primary damping coefficient, respectively.  $y$  represents the displacement of the base, and  $x_a$  and  $x_p$  represent the displacement of the NES mass relative to the base and that of the primary mass relative to the base, respectively. The equations of motion of the system are given as

$$m_p \ddot{x}_p + c_p \dot{x}_p + k_p x_p - c_{am} \dot{z} - k_1 z - k_3 z^3 = -m_p \ddot{y}, \quad (1)$$

$$m_a (\ddot{x}_p + \ddot{z}) + c_{am} \dot{z} + k_1 z + k_3 z^3 + c_{ae} (\dot{x}_p + \dot{z}) = -m_a \ddot{y}, \quad (2)$$

where  $z = x_a - x_p$  is the displacement of the NES mass relative to the primary mass. Assuming the base motion is harmonic, then the base acceleration is given by  $\ddot{y} = -A_y \cos(\Omega t)$ , where  $A_y = \Omega^2 Y$  is the amplitude of the acceleration,  $\Omega$  is the excitation frequency, and  $Y$  is the amplitude of the base motion. Equations (1) and (2) can be reformulated as

$$\ddot{x}_p + 2\zeta_p \omega_p \dot{x}_p + \omega_p^2 x_p - 2\mu \zeta_{am} \omega_a \dot{z} - \mu \omega_a^2 (z + \lambda z^3) = -\ddot{y}, \quad (3)$$

$$\ddot{z} - 2(\zeta_p \omega_p - \zeta_{ae} \omega_a) \dot{x}_p - \omega_p^2 x_p + 2\omega_a [(1 + \mu)\zeta_{am} + \zeta_{ae}] \dot{z} + \omega_a^2 (1 + \mu)(z + \lambda z^3) = 0, \quad (4)$$

where

$$\omega_p = \sqrt{\frac{k_p}{m_p}}, \omega_a = \sqrt{\frac{k_1}{m_a}}, \mu = \frac{m_a}{m_p}, \lambda = \frac{k_3}{k_1}, \zeta_p = \frac{c_p}{2m_p \omega_p}, \quad (5)$$

$$\zeta_{am} = \frac{c_{am}}{2m_a \omega_a}, \zeta_{ae} = \frac{c_{ae}}{2m_a \omega_a}.$$

Based on the results from the system characterization [19], the parameter values used in the following simulation are  $\omega_p = 60.457$  rad/s,  $\omega_a = 24.183$  rad/s,  $\mu = 0.177$ ,  $\lambda = 9.765 \times 10^4$  m<sup>2</sup>,  $\zeta_p = 7.3 \times 10^{-3}$ ,  $\zeta_{am} = 4.1 \times 10^{-3}$ .

Fig. 4 shows the circuit of the electromagnetic energy harvester where  $R_{coil}$  and  $L_{coil}$  are the resistance and inductance of one coil, respectively, and  $R_{load}$  is the resistance of the load resistor. As the impedance due to the inductance of the coils is negligible, the electromagnetic energy harvester is equivalent to an electromagnetic damper with a damping coefficient

$$c_{ae} = \frac{\Theta^2}{2R_{coil} + R_{load}}, \quad (6)$$

where  $\Theta$  is the transduction factor that is approximated to be a constant. The value of  $\zeta_{ae}$  varies with  $c_{ae}$ . In [18], the transduction factor was found to be  $\Theta = 2.596$  Tm and the coil resistance is measured as  $R_{coil} = 2.3 \Omega$ .

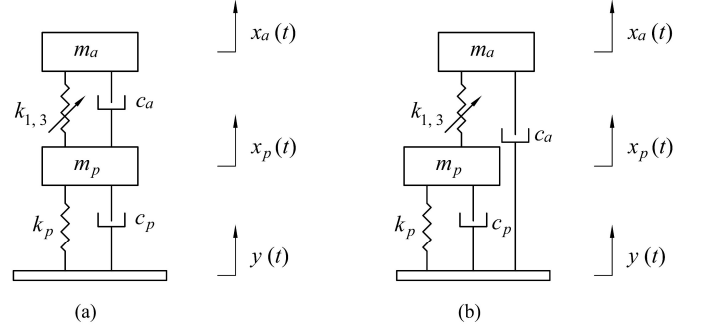


Figure 1. Two different ways to attach a variant NES's damper: (a) traditional way; (b) non-traditional way.

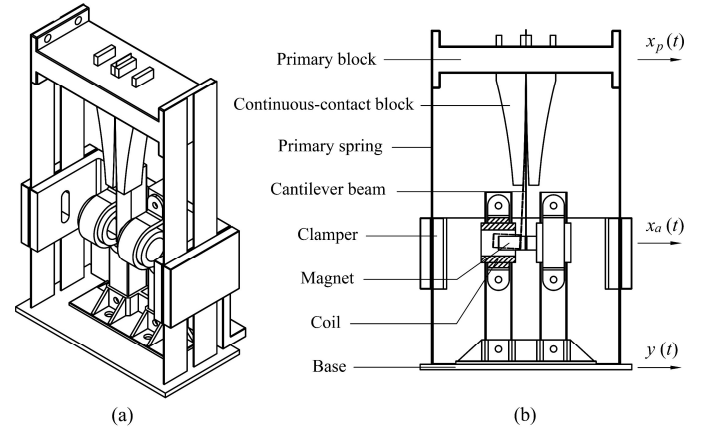


Figure 2. The CAD drawings of the developed apparatus: (a) isometric view; (b) front view.

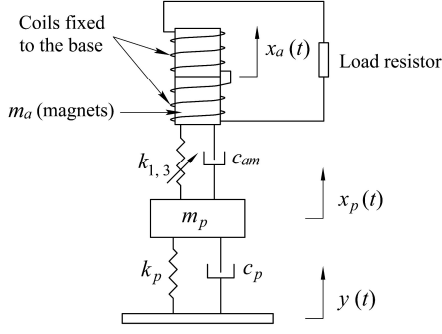


Figure 3. Dynamic model of the developed apparatus.

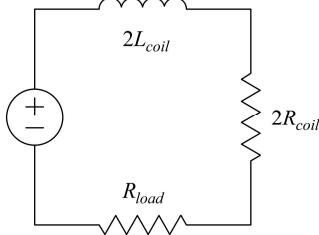


Figure 4. Circuit of the energy harvester.

### III. HARMONIC BALANCE METHOD

In terms of predicting the steady-state response of nonlinear systems, the harmonic balance (HB) method is more efficient than numerical simulation in time domain since the latter has to compute many cycles in order to generate the steady-state response, and such process can be time-consuming [20]. In order to apply the HB method to (3) and (4), the following state variables are defined:

$$x_1 = x_p, x_2 = z, x_3 = \dot{x}_p, x_4 = \dot{z}. \quad (7)$$

With the assumption that the predominant component of the steady-state response has the same frequency as that of the excitation, the equations of motion of the system can be written in the form of  $\dot{\vec{x}} = \vec{f}(t, \vec{x}) = \vec{f}(t + T, \vec{x})$ .

$$\begin{aligned} \dot{x}_1 &= x_3, \\ \dot{x}_2 &= x_4, \\ \dot{x}_3 &= -2\zeta_p \omega_p x_3 - \omega_p^2 x_1 + 2\mu\zeta_{am} \omega_a x_4 + \mu\omega_a^2 (x_2 + \lambda x_2^3) \\ &\quad + A_y \cos \Omega t, \\ \dot{x}_4 &= 2(\zeta_p \omega_p - \zeta_{ae} \omega_a) x_3 + \omega_p^2 x_1 - 2\omega_a [(1 + \mu)\zeta_{am} + \zeta_{ae}] x_4 \\ &\quad - \omega_a^2 (1 + \mu)(x_2 + \lambda x_2^3). \end{aligned} \quad (8)$$

The truncated Fourier series of the assumed solution are

$$\vec{\hat{x}}(t) = \vec{a} + \mathbf{A}\vec{c}(t) + \mathbf{B}\vec{s}(t), \quad (9)$$

which can be written in component form as

$$\begin{aligned} \hat{x}_i(t) &= a_i + \sum_{n=1}^N [A_{in} c_n(t) + B_{in} s_n(t)], \\ i &= 1, 2, \dots, D, n = 1, 2, \dots, N, \end{aligned} \quad (10)$$

where  $a_i$ ,  $A_{in}$ , and  $B_{in}$  are constants,  $c_n(t) = \cos(n\Omega t)$  and  $s_n(t) = \sin(n\Omega t)$  are the harmonics,  $D = 4$  is the dimension of the system, and  $N$  is the number of harmonics. As the system under consideration has a nonlinear stiffness with a cubic term,  $N = 3$  is used in this study. The residual function in vector form is defined by

$$\vec{r}(t) = \vec{f}(t, \vec{\hat{x}}(t)) - \dot{\vec{\hat{x}}}(t). \quad (11)$$

Minimizing the residual functions using the Galerkin method yields

$$\begin{aligned} r_i^{\vec{a}}(\vec{a}, \mathbf{A}, \mathbf{B}) &= \frac{1}{T} \int_0^T \vec{r}(t) dt = 0, \\ R_{in}^{\mathbf{A}}(\vec{a}, \mathbf{A}, \mathbf{B}) &= \frac{1}{T} \int_0^T \vec{r}(t) \vec{c}^T(t) dt = 0, \\ R_{in}^{\mathbf{B}}(\vec{a}, \mathbf{A}, \mathbf{B}) &= \frac{1}{T} \int_0^T \vec{r}(t) \vec{s}^T(t) dt = 0. \end{aligned} \quad (12)$$

The above step generates a system of  $D(2N + 1)$ , i.e.  $4 \times (2 \times 3 + 1) = 28$  equations with the same number of unknowns that can be solved by the Newton-Raphson method.

### IV. SIMULATION RESULTS

In the following simulations, the identified parameter values given in section II are used. The results by the HB method are used to generate the so-called frequency response plot (FRP) [21]. Figs. 5 and 6 show the FRPs with a load resistance of  $R_{load} = 20 \Omega$  under two excitation levels  $A_y = 1 \text{ m/s}^2$  and  $A_y = 1.5 \text{ m/s}^2$ , respectively. The blue solid line represents the up-sweep responses of the primary system attached with the non-traditional variant NES while the red dashed line represents the down-sweep ones. The green line shows the frequency response of the primary system alone. It can be seen that the variant NES can suppress vibration of the primary system in a wide frequency region effectively. The effectiveness of the vibration suppression deteriorates with an increase of the excitation level. As shown in Figs. 5 and 6, the amplitude of the responses of the nonlinear systems jumps up or down abruptly at some specific frequencies. This phenomenon is referred to as the amplitude jump, which is a typical behavior of nonlinear systems [22]. With an up-sweep excitation, the jump frequencies with  $A_y = 1 \text{ m/s}^2$  are around 7.0 Hz and 10.7 Hz, while the jump frequencies with  $A_y = 1.5 \text{ m/s}^2$  are around 7.7 Hz and 11.2 Hz. With a down-sweep excitation, the jump frequencies with  $A_y = 1 \text{ m/s}^2$  are around 9.8 Hz and 5.9 Hz, while the jump frequencies with  $A_y = 1.5 \text{ m/s}^2$  are around 10.0 Hz and 6.7 Hz.

In order to verify the approximate steady-state responses by the HB method, the solution of (8) under a slow frequency sweep excitation is numerically obtained by using the MATLAB function ode45. To this end, the excitation frequency  $f = \Omega/2\pi$  is varied by

$$f = f_s + \frac{f_e - f_s}{T_d} t = f_s + rt, \quad (13)$$

where  $f_s$  is the starting frequency,  $f_e$  is the ending frequency,  $T_d$  is the sweep duration, and  $r$  is the sweeping rate. In this study,  $f_s$

is set to be 2 Hz and 20 Hz in an up-sweep and a down-sweep, respectively,  $f_e$  is set to be 20 Hz and 2 Hz in an up-sweep and a down-sweep, respectively, and  $r$  is set to be 0.02 Hz/s and  $-0.02$  Hz/s in an up-sweep and a down-sweep, respectively.

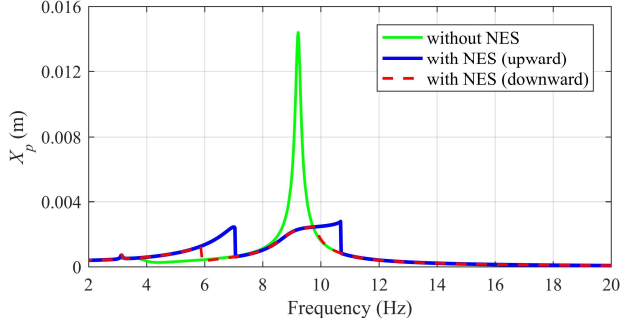


Figure 5. Frequency responses of the primary system from up-sweep and down-sweep excitations with  $A_y = 1 \text{ m/s}^2$  and by HB method.

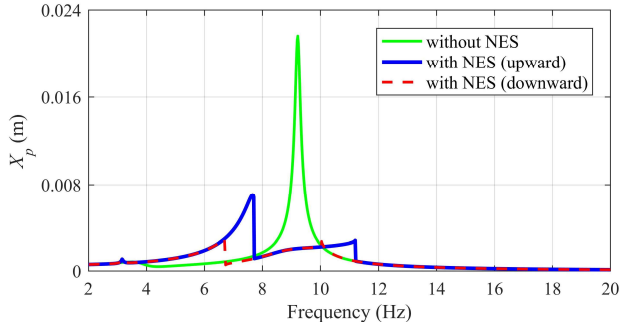


Figure 6. Frequency responses of the primary system from up-sweep and down-sweep excitations with  $A_y = 1.5 \text{ m/s}^2$  by HB method.

In the following simulation, the excitation amplitude of  $A_y = 1 \text{ m/s}^2$  is used. Figs. 7 to 9 show the amplitudes of the steady-state responses of the developed apparatus obtained using the two methods with three different load resistances of  $R_{load} = 20 \Omega$ ,  $100 \Omega$ , and  $200 \Omega$ . Figs. 7(a) to 9(a) show the amplitudes of the steady-state response  $X_p$  of the primary system, while Figs. 7(b) to 9(b) show the amplitudes  $Z$  of the steady-state relative response of the NES. The blue solid lines and the red solid lines represent the up-sweep responses and the down-sweep responses obtained by numerical simulation respectively, and the dashed lines represent the responses obtained by using the HB method. In general, both of the results agree well in terms of the magnitudes and the jump frequencies. Some discrepancies are noted when the load resistance is large or the electric damping is low. This is due to the fact that when the damping is low, the transient responses in the frequency sweep excitation become more noticeable. Table I shows the jump frequencies in the upward and downward FRPs with different load resistances.

Figs. 7 to 9 show that in an up-sweep, the peak value of  $X_p$  at the first jump frequency is significantly increased as the load resistance increases, while the value of  $X_p$  around the second jump frequency remains at the same level. In a down-sweep, the value of  $X_p$  remains low and nearly unchanged as the load resistance increases. It can also be observed from Table I, as well as Figs. 7 to 9 that the unstable regions are widened with an

increase of the load resistance. The observations above indicate that although the nonlinear effect of the system is stronger with a larger load resistance, a lower resistance is preferred for better vibration suppression.

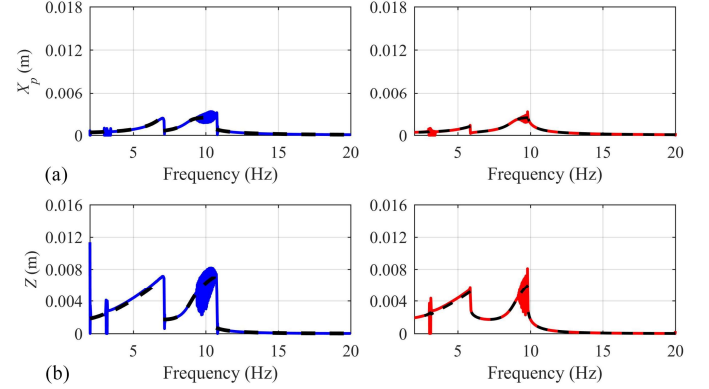


Figure 7. Up-sweep frequency responses (left column) and down-sweep frequency responses (right column) with  $R_{load} = 20 \Omega$ : (a)  $X_p$ ; (b)  $Z$ .

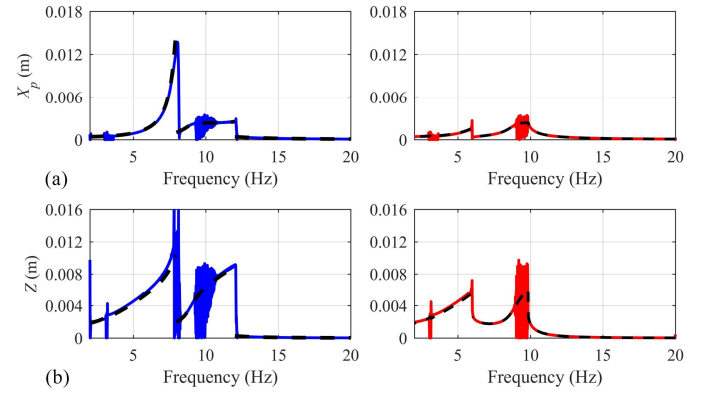


Figure 8. Up-sweep frequency responses (left column) and down-sweep frequency responses (right column) with  $R_{load} = 100 \Omega$ : (a)  $X_p$ ; (b)  $Z$ .

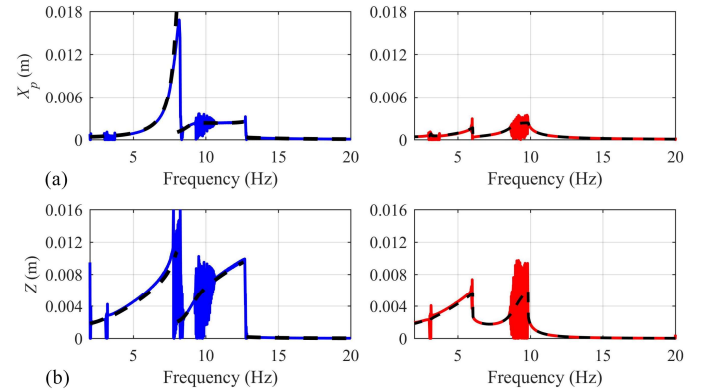


Figure 9. Up-sweep frequency responses (left column) and down-sweep frequency responses (right column) with  $R_{load} = 200 \Omega$ : (a)  $X_p$ ; (b)  $Z$ .

Figs. 10 and 11 show examples of the so-called strongly modulated response (SMR), which is a typical phenomenon of a NES system subjected to harmonic excitation. The SMR is considered as a sign of repeated TET [23, 24]. Figs. 10 and 11 show the time responses with  $R_{load} = 20 \Omega$  and  $200 \Omega$ ,

respectively. Two excitation frequencies of 3.14 Hz and 9.22 Hz are used. Apparently the SMR is established.

TABLE I. JUMP FREQUENCIES WITH DIFFERENT LOAD RESISTANCES.

$R_{load}$	20 $\Omega$	50 $\Omega$	100 $\Omega$	150 $\Omega$	200 $\Omega$
upward	7.04 Hz, 10.68 Hz	7.80 Hz, 11.36 Hz	7.94 Hz, 11.98 Hz	7.98 Hz, 12.40 Hz	8.00 Hz, 12.60 Hz
downward	9.84 Hz, 5.86 Hz	9.86 Hz, 6.00 Hz	9.84 Hz, 5.88 Hz	9.84 Hz, 5.98 Hz	9.84 Hz, 6.02 Hz

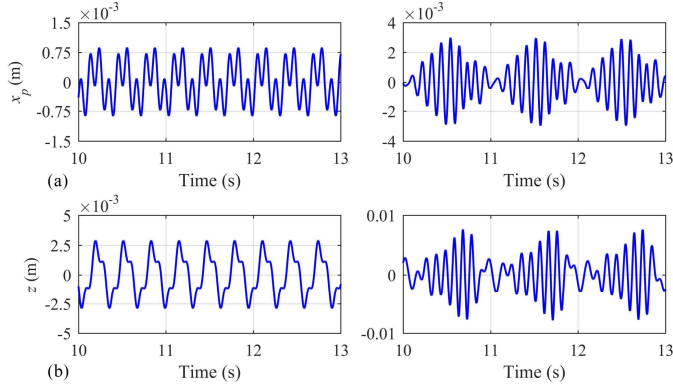


Figure 10. Time responses of SMR with the excitation frequency of 3.14 Hz (left column) and 9.22 Hz (right column) and  $R_{load} = 20 \Omega$ : (a)  $x_p$ ; (b)  $z$ .

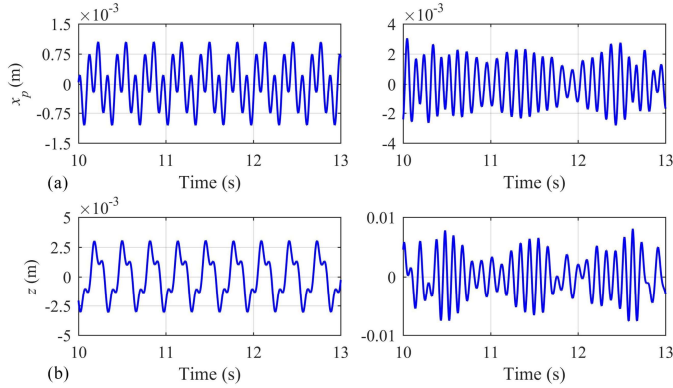


Figure 11. Time responses of SMR with the excitation frequency of 3.14 Hz (left column) and 9.22 Hz (right column) and  $R_{load} = 200 \Omega$ : (a)  $x_p$ ; (b)  $z$ .

With the FRPs obtained, vibration suppression of the developed apparatus with respect to  $R_{load}$  is measured by defining an index which is given by

$$D_3 = \|X_p\|_2, \quad (14)$$

i.e. the second norm of  $X_p$ . This index evaluates the sum of the squared values of  $X_p$ . The lower the value of  $D_3$ , the better the vibration suppression. Fig. 12 shows  $D_3$  with respect to  $R_{load}$  with up-sweep excitation only since  $X_p$  remains nearly unchanged with down-sweep excitation. Clearly, the value of  $D_3$  increases with an increase of  $R_{load}$  in the up-sweep responses, which indicates that a lower  $R_{load}$  is preferred for better vibration suppression.

The energy harvesting efficiency of the system is investigated using the approximate solutions obtained from the HB method. The current in the circuit can be found by [18]

$$i(t) = \frac{\Theta}{2R_{coil} + R_{load}} \dot{x}_a(t). \quad (15)$$

The peak current  $i_{peak}$  is defined by

$$i_{peak} = \frac{\Theta}{2R_{coil} + R_{load}} A, \quad (16)$$

where  $A$  is the peak amplitude of  $\dot{x}_a(t)$ . The value of  $A$  is obtained by generating single-frequency time responses using (10). The peak of the instantaneous power harvested by the load resistor is given as

$$P_{peak} = i_{peak}^2 R_{load}. \quad (17)$$

Fig. 13 shows the peak powers harvested by the load resistor with  $R_{load} = 20 \Omega$ ,  $50 \Omega$ ,  $100 \Omega$ , and  $200 \Omega$ , respectively. As shown in Fig. 13, in terms of the frequency jumping, the overall trends of  $P_{peak}$  with different load resistances are consistent with those seen in the corresponding amplitude-frequency responses. However, in terms of the magnitude, the load resistances have different effects at the two jump frequencies in the up-sweep responses. In Fig. 13(a), at the first jump frequency, the load resistance of  $R_{load} = 50 \Omega$  results in the largest peak power among the four load resistances considered. If the load resistance is further increased, the peak power reduces. At the second jump frequency, the lower the load resistance, the larger the peak power. While in Fig. 13(b), the largest peak power increases at both the jump frequencies with a decrease in  $R_{load}$ .

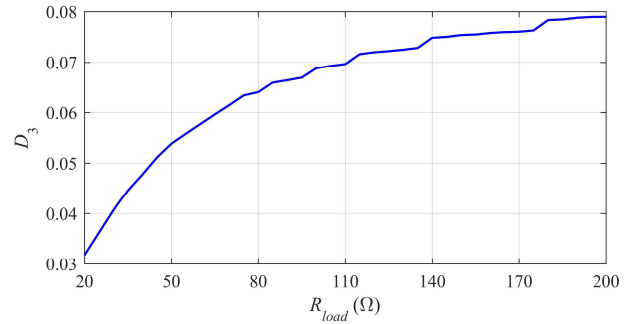


Figure 12.  $D_3$  versus  $R_{load}$ .

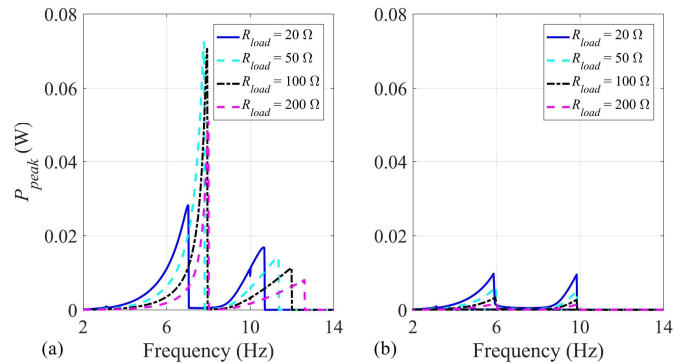


Figure 13. Frequency responses of  $P_{peak}$  with  $R_{load} = 20 \Omega$ ,  $50 \Omega$ ,  $100 \Omega$ , and  $200 \Omega$ : (a) up-sweep; (b) down-sweep.

In order to further investigate the effect of  $R_{load}$  on energy harvesting in the up-sweep responses, the energy harvesting capability of the load resistor in a broad frequency range is measured by defining an index as follows:

$$D_4 = \left\| P_{peak} \right\|_2. \quad (18)$$

This index measures a sum of the squared peak powers in the frequency range of interest. Fig. 14 shows the plot of  $D_4$  with respect to  $R_{load}$  in the up-sweep responses. As shown in Fig. 14, with an increase of  $R_{load}$ , the value of  $D_4$  increases until  $R_{load}$  reaches  $50 \Omega$ , then decreases. In terms of energy harvesting, a load resistance around  $50 \Omega$  is preferred for the system. Based on the trends of  $D_3$  and  $D_4$ , it can be concluded that a proper trade-off between vibration suppression and energy harvesting can be obtained around  $R_{load} = 50 \Omega$ .

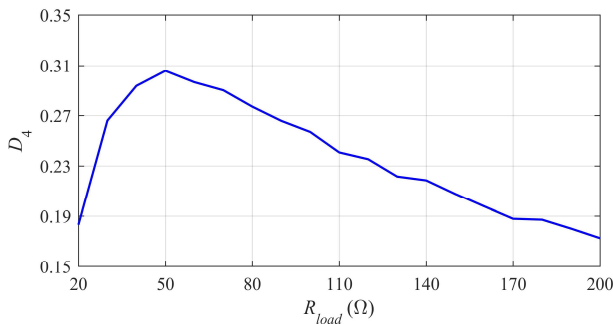


Figure 14.  $D_4$  versus  $R_{load}$ .

## V. CONCLUSION

Harmonically forced responses of a non-traditional variant NES are investigated in this study. The frequency response plots are obtained by using the HB method and the frequency sweep excitation with the MATLAB function ode45. Overall, the results of the two methods agree well. Some typical behaviors of the NES system are observed such as the jump phenomenon and SMR. The peak power harvested by the load resistor is used to investigate the energy harvesting efficiency. The results reveal that vibration suppression can be achieved with a high electric damping, i.e. a small  $R_{load}$ , while energy harvesting can be achieved with a load resistance of around  $50 \Omega$ .

## REFERENCES

- [1] Twiefel, J., & Westermann, H. (2013). Survey on broadband techniques for vibration energy harvesting. *Journal of Intelligent Material and Structures*, 24(11), 1291-1302.
- [2] Yang, Z., Zhou, S., Zu, J., & Inman, D. (2018). High-performance piezoelectric energy harvesters and their applications. *Joule*, 2(4), 642-697.
- [3] Hunt, J. B., & Nissen, J. C. (1982). The broadband dynamic vibration absorber. *Journal of Sound and Vibration*, 83(4), 573-578.
- [4] Nissen, J. C., Popp, K., & Schmalhorst, B. (1985). Optimization of a nonlinear dynamic vibration absorber. *Journal of Sound and Vibration*, 99(1), 149-154.
- [5] Oueini, S. S., & Nayfeh, A. H. (2000). Analysis and application of a nonlinear vibration absorber. *Journal of Vibration Control*, 6(7), 999-1016.

- [6] Gendelman, O., Manevitch, L. I., Vakakis, A. F., & M'Closkey, R. (2001). Energy pumping in nonlinear mechanical oscillators: part I – dynamics of the underlying Hamiltonian systems. *Journal of Applied Mechanics*, 68(1), 4-41.
- [7] Vakakis, A. F. & Gendelman, O. (2001). Energy pumping in nonlinear mechanical oscillators: part II – resonance capture. *Journal of Applied Mechanics*, 68(1), 42-48.
- [8] Vakakis, A. F., Gendelman, O. V., Bergman, L. A., McFarland, D. M., Kerschen, G., & Lee, Y. S. (2008). *Nonlinear Targeted Energy Transfer in Mechanical and Structural Systems*, Springer, New York.
- [9] Nguyen, T. A., Pernot, S. (2011). Design criteria for optimally tuned nonlinear energy sinks—part I: transient regime. *Nonlinear Dynamics*, 69(1), 1-19.
- [10] Ahmadbadi, Z. N., & Khadem, S. E. (2014). Nonlinear vibration control and energy harvesting of a beam using a nonlinear energy sink and a piezoelectric device. *Journal of Sound and Vibration*, 333(19), 4444-4457.
- [11] Fang, Z., Zhang, Y., Li, X., Ding, H., & Chen, L. (2017). Integration of a nonlinear energy sink and a giant magnetostrictive energy harvester. *Journal of Sound and Vibration*, 391, 35-49.
- [12] Kerschen, G., Vakakis, A. F., Lee, Y. S., McFarland, D. M., Kowtko, J. J., & Bergman, L. A. (2005). Energy transfers in a system of two coupled oscillators with essential nonlinearity: 1:1 resonance manifold and transient bridging orbits. *Nonlinear Dynamics*, 42(3), 283-303.
- [13] Kerschen, G., McFarland, D. M., Kowtko, J. J., Lee, Y. S., Bergman, L. A., & Vakakis, A. F. (2007). Experimental demonstration of transient resonance capture in a system of two coupled oscillators with essential stiffness nonlinearity. *Journal of Sound and Vibration*, 299(4), 822-838.
- [14] Gourdon, E., Alexander, N. A., Taylor, C. A., Lamarque, C. H., & Pernot, S. (2007). Nonlinear energy pumping under transient forcing with strongly nonlinear coupling: Theoretical and experimental results. *Journal of Sound and Vibration*, 300(3), 522-551.
- [15] Kremer, D., & Liu, K. (2014). A nonlinear energy sink with an energy harvester: transient response. *Journal of Sound and Vibration*, 333(20), 4859-4880.
- [16] Kremer, D., & Liu, K. (2017). A nonlinear energy sink with an energy harvester: harmonically forced responses. *Journal of Sound and Vibration*, 410, 287-302.
- [17] Zhang, Y., Liu, K., & Tang, L. (2017). Piezoelectric energy harvesting using a nonlinear energy sink. *Journal of Intelligent Material Systems and Structures*, 28(3), 307-322.
- [18] Yuan, M., Liu, K., & Sadhu, A. (2018). Simultaneous vibration suppression and energy harvesting with a non-traditional vibration absorber. *Journal of Intelligent Material Systems and Structures*, 29(8), 1748-1763.
- [19] Jin, Y., Liu, K., Li, D., Xiong, L., & Tang, L. (2019, November). *A non-traditional variant nonlinear energy sink: transient responses*. The Proceedings of the ASME 2019 International Design Engineering Technical Conferences and Computers and Information in Engineering Conference, Anaheim, California.
- [20] Leadenham, S., & Erturk, A. (2014). M-shaped asymmetric nonlinear oscillator for broadband vibration energy harvesting: Harmonic balance analysis and experimental validation. *Journal of Sound and Vibration*, 333(23), 6209-6223.
- [21] Xiong, L., Tang, L., Liu, K., & Mace, B. R. (2018). Broadband piezoelectric vibration energy harvesting using a nonlinear energy sink. *Journal of Physics D: Applied Physics*, 51(18), 185502.
- [22] Parzygnat, W. J., & Pao, Y. (1978). Resonance phenomena in the nonlinear vibration of plates governed by Duffing's equation. *International Journal of Engineering Science*, 16(12), 999-1017.
- [23] Gatti, G., & Brennan, M. J. (2011). On the effects of system parameters on the response of a harmonically excited system consisting of weakly coupled nonlinear and linear oscillators. *Journal of Sound and Vibration*, 330(18), 4538-4550.
- [24] Gatti, G., Kovacic, I., & Brennan, M. J. (2010). On the response of a harmonically excited two degree-of-freedom system consisting of a linear and a nonlinear quasi-zero stiffness oscillator. *Journal of Sound and Vibration*, 329(10), 1823-1835.